J. Fluid Mech. (2011), *vol.* 672, *pp.* 451–476.
doi:10.1017/S0022112010006105

Steady longitudinal vortices in supersonic turbulent separated flows

ERICH SCHÜLEIN[1]† AND VICTOR M. TROFIMOV[2]

[1]Department of High Speed Configurations, German Aerospace Center DLR, Institute of Aerodynamics and Flow Technology, Bunsenstr. 10, 37073 Göttingen, Germany

[2]Department of Technology, Novosibirsk State Pedagogical University, ul. Viluyskay 28, 630126 Novosibirsk, Russia

(Received 4 March 2010; revised 30 October 2010; accepted 20 November 2010)

Large-scale longitudinal vortices in high-speed turbulent separated flows caused by relatively small irregularities at the model leading edges or at the model surfaces are investigated in this paper. Oil-flow visualization and infrared thermography techniques were applied in the wind tunnel tests at Mach numbers 3 and 5 to investigate the nominally 2-D ramp flow at deflection angles of 20°, 25° and 30°. The surface contour anomalies have been artificially simulated by very thin strips (vortex generators) of different shapes and thicknesses attached to the model surface. It is shown that the introduced streamwise vortical disturbances survive over very large downstream distances of the order of 10^4 vortex-generator heights in turbulent supersonic flows without pressure gradients. It is demonstrated that each vortex pair induced in the reattachment region of the ramp is definitely a child of a vortex pair, which was generated originally, for instance, by the small roughness element near the leading edge. The dependence of the spacing and intensity of the observed longitudinal vortices on the introduced disturbances (thickness and spanwise size of vortex generators) and on the flow parameters (Reynolds numbers, boundary-layer thickness, compression corner angles, etc.) has been shown experimentally.

Key words: boundary-layer separation, free shear layers, high-speed flow

1. Introduction

Streamwise vortices are frequently companions of various external and internal flows resulting in distinct cross-flow variations in surface heat, shear stress and pressure loads. The importance of studying such vortices is based not only on these effects being significant for practical applications, but also on entirely fundamental interest in flows with complicated topological evolution. Especially in fully turbulent flows, this phenomenon gives a challenging example of unexpected long-term preservation and development of disturbances in boundary layers.

It is well known that steady longitudinal vortices can be evoked by any noticeable discontinuities at the leading edges or in the vicinity of obstacles on the surfaces (Pearcey 1961). The pioneering investigations by Ginoux (see Ginoux 1958, 1960, 1969, 1971) showed that not only macro irregularities at the leading edges, but also smallest micro discontinuities or notches could lead to such vortices in laminar flows.

† Email address for correspondence: erich.schuelein@dlr.de

The existence of counter-rotating streamwise vortices in regions with adverse pressure gradients in cases with and without flow separation was demonstrated in the cited works by surface flow visualizations and flow-field measurements.

The explanation for the nature of this phenomenon used most often is based on Görtler's theoretical results (see Görtler 1940, 1941). His physical model predicts the formation of longitudinal counter-rotating vortices in flows with concave streamline curvature evoked through centrifugal instability. The wall curvature is really not necessary for this. The observations of these vortices in laminar flows on a planar surface downstream of the incident shock-induced separation and reattachment (e.g. Henckels, Kreins & Maurer 1993; Domröse, Krause & Meinke 1996; Kreins, Henckels & Maurer 1996) have shown that the streamline curvature, necessary to produce Görtler-like vortices, emerges due to the reattachment of the free shear layer. This concave curvature controls the intensity of the vortices and consequently the level of typical local heat flux peaks in the reattachment region and downstream of it.

Although a large number of different experimental studies, in which clear manifestations of such (unintended) large-scale longitudinal vortices in turbulent separated flows were obtained (see Maurer 1966; Roshko & Thomke 1966; Brazhko 1979; Zheltovodov *et al.* 1985; Trofimov & Shtrekalkin 1990), their existence has long been controversial (e.g. Vermeulen & Simeonides 1992; Simeonides 1993). The reason is that the long-term preservation of longitudinal disturbances in turbulent flows seems to be in contradiction to the common-justified view of the turbulence as a stochastic system that is 'unrepeatable in detail' and 'irregular in both time and space' (Falkovich & Sreenivasan 2006).

The generation of vortices in turbulent flows is usually thought to result from the mean motion, while downstream their subsequent fragmentation into smaller vortices occurs, leading finally to the dissipation of the kinetic energy into heat at smallest possible length scales determined above all by the fluid viscosity. This process can be described as a 'cascade', since the generation of smaller scales increases rapidly as the scale size decreases (e.g. Falkovich & Sreenivasan 2006), and is expected to actuate the dissipation of disturbances induced, for instance, by a vortex generator (e.g. Lin 2002).

Some simplified model ideas about the turbulent-flow constitution are devastated by the findings of the past years. So, in turbulent flows, situations are known in which an 'inverse cascade' of turbulent energy occurs. This type of energy transformation occurs in two-dimensional (2-D) ocean turbulence, where it seems to give rise to gigantic vortices (Kraichnan 1973). The same process, which can be adequately predicted by the model of helical atmospheric turbulence, is most likely to accompany the emergence of hurricanes and typhoons (see Moiseev *et al.* 1983; Berezin, Hutter & Zhukov 1991; Berezin & Trofimov 1996). In all these cases, turbulent vortices seem to transfer energy in the opposite direction, from small to larger vortices.

Moreover, recent studies accomplished by means of modern high-resolution measurement techniques show the existence of elongated superstructures in zero-pressure-gradient turbulent boundary layers, which are noticeable in large-scale (or even very-large-scale) stripiness in the streamwise velocity fluctuations (e.g. Tomkins & Adrian 2003; Ganapathisubramani, Clemens & Dolling 2006; Hutchins & Marusic 2007). These longitudinal unsteady coherent structures with lengths greater than 40δ (see Ganapathisubramani *et al.* 2006) could be observed in different incompressible and compressible undisturbed wall-bounded turbulent flows (Marusic *et al.* 2010). The spanwise meandering motion of these coherent superstructures (Hutchins & Marusic 2007) is most likely the reason why they remained invisible to single-point measurement techniques used in the past. Although their origin and nature remain

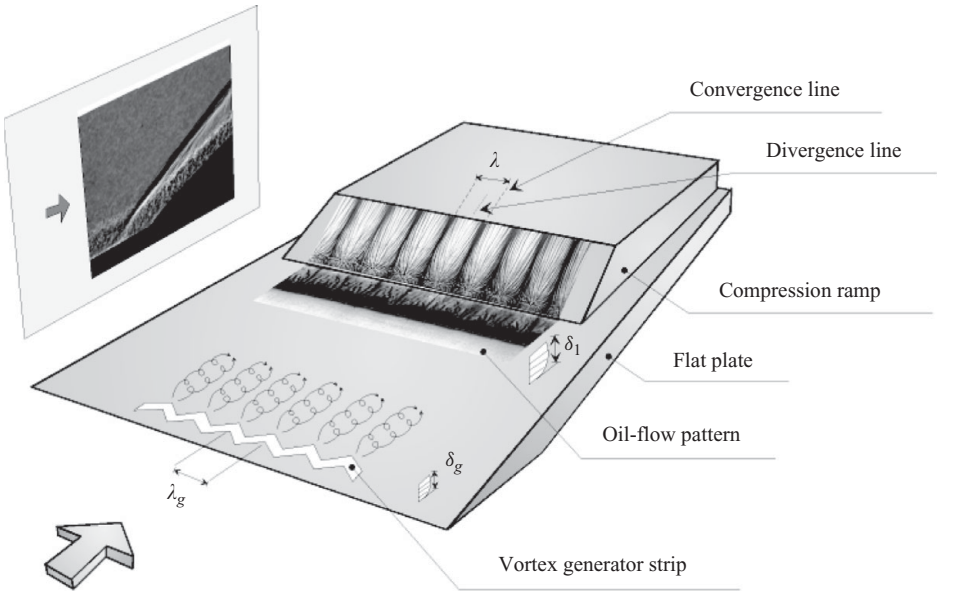

FIGURE 1. Sketch of the test model investigated by Schülein (2002), with obtained shadowgraph image and oil-flow pattern.

mostly unexplored, the unexpected long conservation of such coherent structures in zero-pressure gradient turbulent flows seems to be a very important finding that can help to reassess some established model ideas about the evolution of disturbances in turbulent flows. It is really unclear whether or not a relation exists between the meandering superstructures detected in zero-pressure-gradient turbulent boundary layers and the quasi-steady longitudinal vortices evoked through centrifugal instability.

The other open question in this context is the role of the laminar–turbulent transition process in the formation of meandering superstructures or steady longitudinal vortices observed in fully developed turbulent flows. It is well known, for example, that isolated roughness elements or smallest leading-edge discontinuities cause early boundary-layer transition (see e.g. Schneider 2007) accompanied by formation of turbulent wedges, extending downstream into the ambient laminar flow and leading to evidence of secondary flows due to the displacement effect. Is it possible that the laminar-boundary-layer tripping is the preliminary event, leading to the generation of large-scale longitudinal vortices (or streaky structures) downstream in turbulent boundary layers? These questions remain to be answered.

The present work is a continuation of the experimental investigations performed by Schülein (2002), where the possibility of artificial generation of longitudinal vortices in fully turbulent separated flows by very weak disturbances was demonstrated in wind tunnel tests. These previous experiments were conducted in the Ludwieg Tube Facility at DLR Göttingen at a Mach number of $M_\infty = 3$ and a Reynolds number of $Re_x = 9 \times 10^6$ on a 20° compression corner model (figure 1). The obtained results have clearly proved that by thorough preparation of the leading edges, the footprints of steady large-scale streamwise vortices in the reattachment region on a compression wedge installed on a flat plate can be completely eliminated: the limiting streamline pattern displays a quite 2-D turbulent mean flow (figure 2*a*).

When some periodical (equally spaced) low-profile vortex generators (LPVG) or zigzag strips from self-adhesive 30–50 μm-thin foil were mounted near the leading

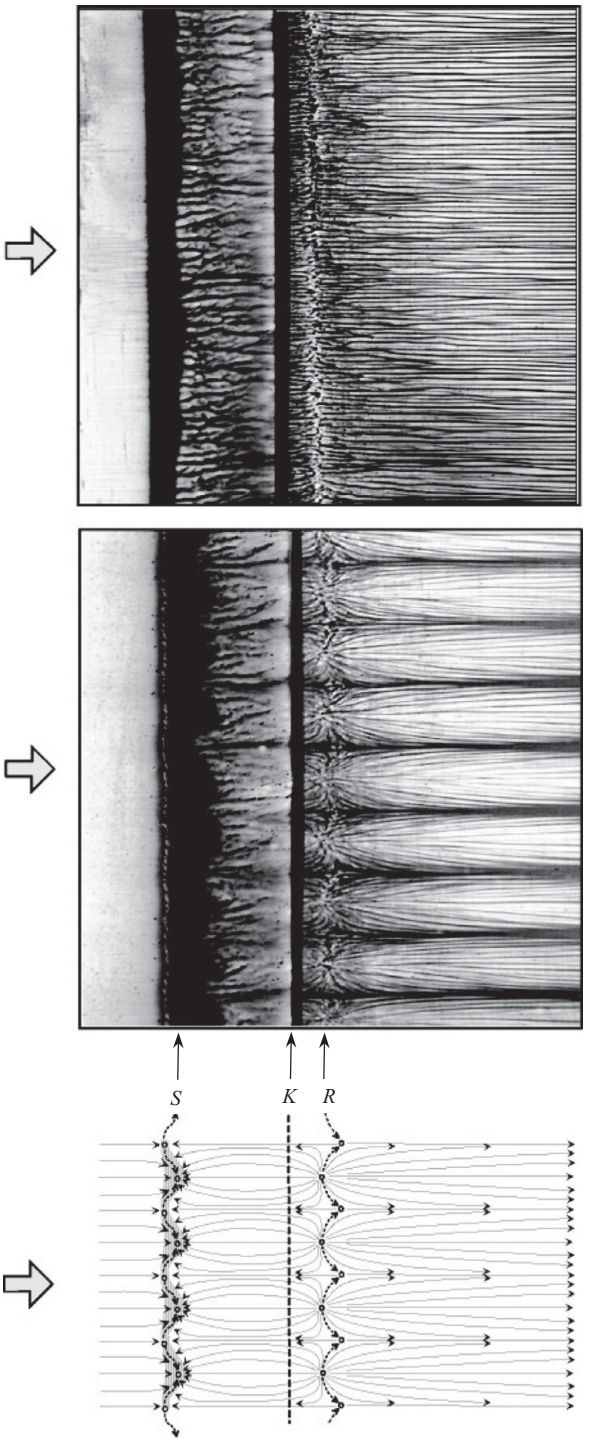

FIGURE 2. Flow pattern in the vicinity of the 20°-compression corner at Mach 3 (Schülein 2002): (*a*) flow without vortex generators; (*b*) flow with artificially generated longitudinal vortices; (*c*) sketch of the skin-friction pattern. *S* and *R* are the ramp-flow separation and reattachment lines, *K* denotes the kink of the model (leading edge of the compression ramp with $x = x_s$).

edge of the flat plate, the footprints of the large-scale longitudinal vortex structures were observed in the reattachment region at distances up to over 10^4 thicknesses of the vortex generator (figure 2*b*). The z-coordinates of the common longitudinal axis of each induced steady vortex pair observed agree exactly with those of the rearmost points of the zigzag-strip trailing edges (teeth-tips). Moreover, for all investigated vortex generators, the vortex-pair structures observed show always a common divergence line along this axis. It is very important to note that the transversal size of the generated vortex pairs λ, often called vortex wavelength or vortex-pair spacing below, can be different from the vortex-generator wavelength λ_g defined in this work as teeth spacing of the used periodical VG-strips (see figure 1).

Extensive numerical studies conducted by Lüdeke (2003) with the Reynolds-averaged Navier–Stokes Code CEVCATS-N for the same model geometry and flow conditions could confirm this behaviour in most details. With the help of both experimental and numerical examinations, some properties of fully turbulent separated flows with forced steady longitudinal vortices were analysed by Lüdeke & Schülein (2002) and by Lüdeke, Radespiel & Schülein (2004). However, some discrepancies between these numerical and experimental results were found.

First of all, contrary to the experimental observations, the properties simulated numerically show a transverse shift (phase shift) in the location of longitudinal vortices downstream of the VGs. In all cases studied numerically, the induced counter-rotating vortex pairs are characterized by a common convergence line downstream of each teeth-tip. The vortex pairs observed experimentally exhibit a common divergence line along these virtual axes.

The second important discrepancy regards the free wavelength of generated vortices λ. In this case, the variation of the generator-to-generator or teeth-to-teeth spacing λ_g in the wind tunnel tests clearly showed that the generated vortex pairs have always retained a certain common wavelength λ and are not free scalable at fixed flow conditions. For a wavelength λ_g of the disturbance that is essentially bigger than the characteristic wavelength of the vortex pair λ, the gap between neighbouring ones showed no footprints of large-scale longitudinal vortices. This critical value of the VG spacing corresponds to the dominant wavelength λ of the induced longitudinal vortices, which is approximately equal to the incoming boundary-layer thickness immediately upstream of the separation zone. Contrary to these experimental observations, the cited numerical results show only a weakening of the vortex effects for bigger generator-to-generator spacing, but not the formation of spanwise-bounded vortices, which fill only a part of the distance between two neighbouring vortex generators. In other words, the wavelength of generated vortex pairs λ in the numerical tests is always equal to the generator-to-generator spacing λ_g.

The aim of the present work is to examine the fact of a natural wavelength of the artificial forced streamwise vortices, which grows with the boundary-layer thickness depending on the other crucial parameters. The disagreement of the experimental and numerical results have additionally stimulated this new experimental study. The results obtained were initially presented by Schülein & Trofimov (2007) at the 1st CEAS European Air & Space Congress.

2. Experimental program

2.1. *Wind tunnel, test model and flow conditions*

The investigations were conducted in the Ludwieg Tube Facility DNW-RWG at DLR Göttingen. The specific feature of a Ludwieg Tube is the use of a long tube as

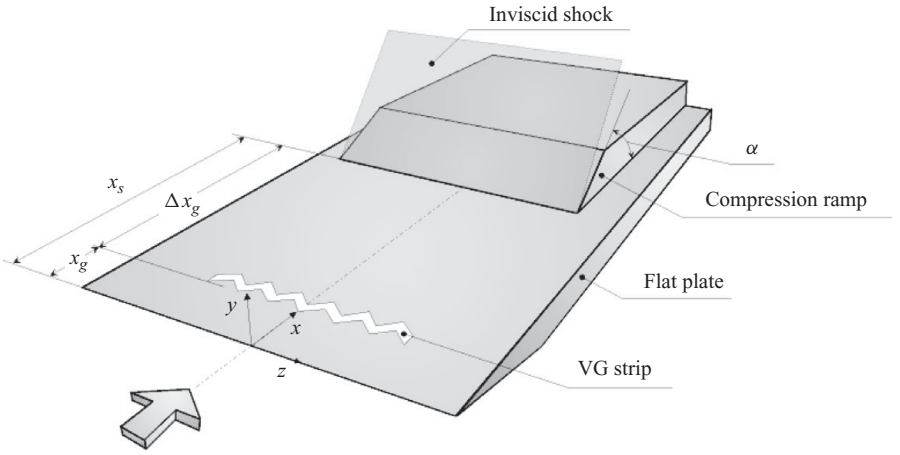

FIGURE 3. Sketch of the test model.

pressure reservoir, which is closed at one end and has a gate valve attached to the other end, followed by a supersonic nozzle, test section and dump tank. After opening the gate valve, the air flow is started by expansion waves, which travel to the closed tube end, are reflected there and travel back. As long as these waves do not reach the nozzle throat, test gas flows out at nearly constant stagnation conditions through the nozzle and the test section into the dump tank. The tube length of 80 m results in a run time of about 300–350 ms. The low operation costs, a relatively large test section and the good optical access make this facility best suited for optical experimental methods and heat flux measurements.

The test model investigated is based on a flat plate with a nominally sharp leading edge that was 500 mm in length and 400 mm in width (figure 3). The compression wedge plate (300 mm in length and 400 mm in width) with deflection angles α of 20°, 25° and 30° could be mounted on the main plate at different locations so that the distance between their leading edges x_s could be varied between 225 mm and 475 mm. The thicknesses of the main plate and the compression wedge plate were 20 mm. The parameters of the investigated model configurations are shown in table 1.

The vortical flow perturbations were artificially forced by very small vortex generators (VGs) placed near the leading edge of the flat plate (see figure 3). The influence of different shapes and dimensions of VGs has been investigated by means of single triangular or rectangular prisms, as well as by means of a row of cylindrical VGs (row of equally spaced dots) (figure 4). The effect of the periodic disturbances was investigated via thin zigzag strips commonly used as turbulator strips. The used vortex generators were made from self-adhesive polyethylene or aluminium foils with constant thicknesses h_g ranging from 0.004 up to 0.4 mm located at different distances x_g from the model's leading edge (figure 3). The parameters of the investigated vortex generator configurations are summarized in table 2.

Two different free-stream flow conditions at Mach numbers 3 and 5 were investigated in the present tests. At $M_\infty = 3$, the nominal conditions in the test section were stagnation temperature $T_0 = 260$ K, stagnation pressure $P_0 = 0.32$ MPa and unit Reynolds number $Re_1 = 30 \times 10^6$/m; and at $M_\infty = 5$, $T_0 = 410$ K, $P_0 = 2.55$ MPa and $Re_1 = 45 \times 10^6$/m. The former measurements of the boundary-layer properties on the flat plate model without VG strips and the compression ramp (Schülein 1999, 2006) showed a well-developed, 2-D turbulent boundary layer at all investigated flow

Distance x_s (mm)	Ramp angle α (deg.)	Model configuration	Mach number M_∞
225	0	A0	3 & 5
275	0	B0	3 & 5
325	0	C0	3 & 5
375	0	D0	3 & 5
425	0	E0	3 & 5
475	0	F0	3 & 5
225	20	A20	3 & 5
275	20	B20	3 & 5
325	20	C20	3 & 5
375	20	D20	3 & 5
425	20	E20	3 & 5
475	20	F20	3 & 5
225	25	A25	3 & 5
275	25	B25	3 & 5
325	25	C25	3 & 5
375	25	D25	3 & 5
425	25	E25	3 & 5
475	25	F25	3 & 5
225	30	A30	5
275	30	B30	5
325	30	C30	5
375	30	D30	5
425	30	E30	5
475	30	F30	5

TABLE 1. Summary of the investigated model configurations.

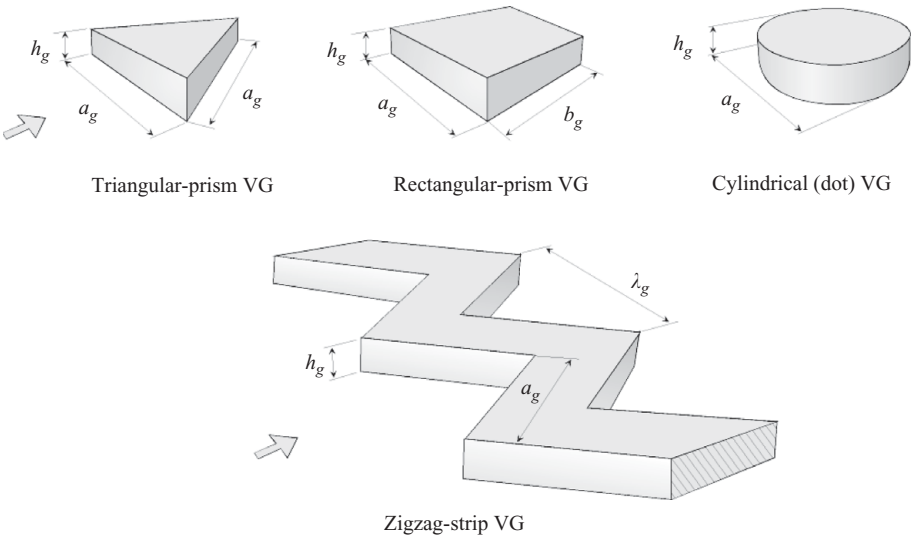

FIGURE 4. Sketch of the low-profile vortex generators investigated.

conditions and distances x_s. In table 3, taken as an example, some undisturbed flat-plate boundary-layer parameters at different distances x from the plate's leading edge at $M_\infty = 5$ and $Re_{1\infty} = 39 \times 10^6$ m^{-1} obtained by Schülein, Krogmann & Stanewsky (1996) are presented. The parameters δ, δ^* and θ correspond to the thicknesses

Parameter varied	Spacing λ_g (mm)	Size a_g (mm)	Thickness h_g (mm)	Distance x_g (mm)	VG type
λ_g effect	2.8	2.0	0.05	10.0	Zigzag strip
	4.2	3.0	0.05	10.0	
	4.9	3.5	0.05	10.0	
	5.7	4.0	0.05	10.0	
	7.1	5.0	0.05	10.0	
	8.5	6.0	0.05	10.0	
	11.3	8.0	0.05	10.0	
	14.1	10.0	0.05	10.0	
	2.8	2.0	0.20	5.0	Zigzag strip
	4.9	3.5	0.20	5.0	
	7.1	5.0	0.20	5.0	
	11.3	10.0	0.20	5.0	
	2.5	1.0	0.10	7.0	Row of dots
	5.0	1.0	0.10	7.0	
	10.0	1.0	0.10	7.0	
	20.0	1.0	0.10	7.0	
	2.5	1.0	0.15	7.0	Row of dots
	5.0	1.0	0.15	7.0	
	10.0	1.0	0.15	7.0	
	20.0	1.0	0.15	7.0	
h_g and x_g effect	∞	5.0	0.05	5.0	Triangular prism
	∞	5.0	0.10	5.0	
	∞	5.0	0.20	5.0	
	∞	3.5	0.004	10.0	Triangular prism
	∞	3.5	0.012	10.0	
	∞	3.5	0.020	10.0	
	∞	3.5	0.028	10.0	
	∞	3.5	0.040	10.0	
	∞	3.5	0.050	10.0	
	∞	5.0	0.05	75.0	Triangular prism
	∞	5.0	0.20	75.0	
	∞	5.0	0.40	75.0	
a_g effect	∞	6.0	0.05	5.0	Triangular prism
	∞	17.0	0.05	5.0	
	22.5	1.0	0.05	10.0	Zigzag strip
	22.5	2.0	0.05	10.0	
	22.5	5.0	0.05	10.0	
δ_1 effect	11.3	10.0	0.05	5.0	Zigzag strip
	11.3	10.0	0.20	5.0	
	∞	7.0	0.05	5.0	Triangular prism

TABLE 2. Summary of the investigated vortex-generator parameters.

($U_\delta = 0.99U_e$), the displacement thickness and the momentum thickness of the mean-flow boundary layer.

2.2. *Measurement techniques*

The investigations were primarily based on the visualization of the surface streamlines with the help of a very liquid mixture of low-viscosity mineral oil with TiO_2 powder. The oil-flow visualization certainly belongs among the simplest but most important experimental techniques for this kind of investigation. This technique

Distance x (mm)	Thickness δ (mm)	Thickness δ^* (mm)	Thickness θ (mm)	Coefficient c_f
266	3.84	1.654	0.159	0.001440
296	4.10	1.786	0.178	0.001341
316	4.41	1.792	0.177	0.001324
336	4.60	1.892	0.189	0.001311
356	4.81	2.000	0.202	0.001294

TABLE 3. Undisturbed flat-plate boundary-layer parameters (without vortex generators) at $M_\infty = 5$ and $Re_{1\infty} = 39 \times 10^6$ m^{-1} from Schülein *et al.* (1996).

offers considerable advantages in revealing fine flow features over other experimental methods with poorer spatial resolution. The dark surface of the test model provides a background with high contrast for the white oil-paint mixture used. For more contrast and clear reproductions, the negative pictures were included in the paper. The oil-flow pictures were recorded during the run by a digital CCD camera with 30 frames s^{-1} and an exposure time of 10 ms. The correct interpretation of the oil-flow pattern is provided thanks to a sequential acquisition and high spatial resolution of pictures.

For the heat transfer measurements, the quantitative infrared thermography (QIRT) technique was applied. For this purpose, the model insert was fabricated from black Plexiglas with a low thermal conductivity. The measurements were made with a real-time infrared camera FLIR SC500 at a frame rate of 60 Hz. Optical access to the test section in the Ludwieg Tube Facility is provided through a custom-built anti-reflection-coated germanium window. The time history of the surface temperature was recorded during the wind tunnel test and then used to determine the local heat flux densities $\dot{q}$, assuming a semi-infinite wall thickness. More details of the QIRT technique used can be found in Schülein (2006).

3. Results and discussion

3.1. *Flat-plate reference flow with and without vortex generators*

The aim of the first part of the investigations was mainly the detection of surface footprints in the incoming boundary layer upstream of the separation zone, which stem from disturbances artificially induced by vortex generators. The measurements by infrared thermography were conducted to compare the heat flux distributions on the basic flat plate with and without vortex generator strips. For these tests, the compression ramp was completely removed from the model.

Figure 5 shows the results of heat flux measurements on the flat plate with and without vortex generators at a Mach number of 5. The heat flux distribution was obtained in two separate wind tunnel runs and covers a total area of about $95 \times 140\,\text{mm}^2$. The heat flux rates here are normalized by a reference value $\dot{q}_1$ indicated in the caption of the figure. The colour scales used in both pictures are identical, allowing a direct comparison of the results. The flow direction is from left to right.

It can be seen that the heating rates without vortex generators (figure 5*a*) decrease monotonically with the distance from the plate's leading edge as expected for equilibrium turbulent boundary-layer flows. Some unevenness in the spanwise direction is originated by residual leading-edge and free-stream irregularities. The

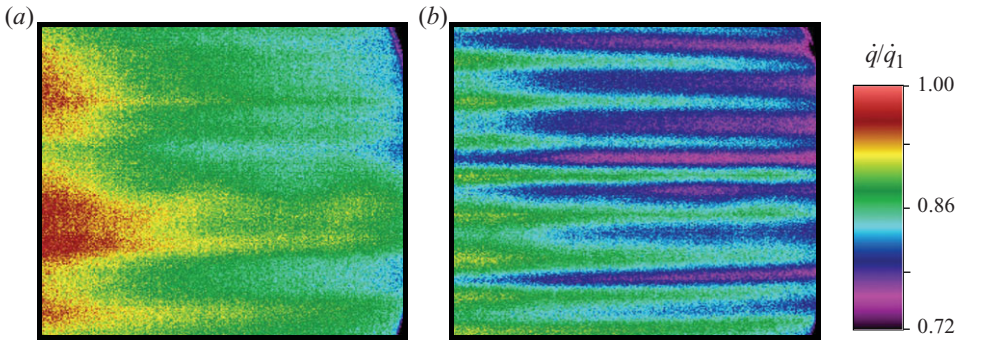

FIGURE 5. Heat flux ratio distribution on the flat plate without a ramp at $M_\infty = 5$ with $\dot{q}_1 = 11800\ \mathrm{W\,m^{-2}}$: (*a*) without vortex generators, and (*b*) with strip-LPVG ($x_g = 5\,\mathrm{mm}$, $h_g = 0.2\,\mathrm{mm}$, $\lambda_g = 11.3\,\mathrm{mm}$). The presented part of the flat-plate surface corresponds to a range of Re_x from 15.6×10^6 to 22.0×10^6.

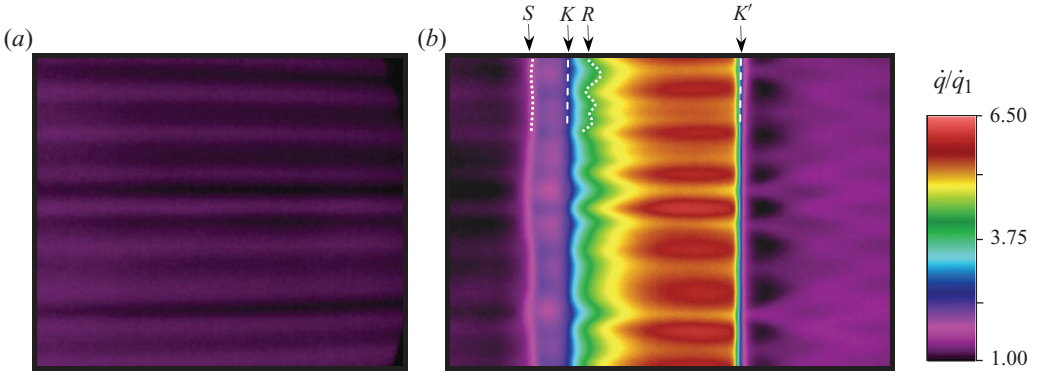

FIGURE 6. Heat flux ratio distribution at $M_\infty = 5$ with a strip-LPVG ($x_g = 5\,\mathrm{mm}$, $h_g = 0.2\,\mathrm{mm}$, $\lambda_g = 11.3\,\mathrm{mm}$) and $\dot{q}_1 = 11\,800\ \mathrm{W\,m^{-2}}$: (*a*) on the flat plate (model E0, the same as in figure 5*b*), and (*b*) on compression corner 25° at $x_s = 425\,\mathrm{mm}$ (model E25, $Re_x = 19.6 \times 10^6$). S and R denote the ramp-flow separation and reattachment lines; K and K' show the first and second kink of the model surface (leading and trailing edge of the compression ramp).

results of heat flux measurements at the same flat plate in the presence of leading-edge zigzag generator strips show (figure 5*b*) distinct footprints of induced longitudinal structures. It is important to note that the oil-flow visualization applied to these configurations did not show any comparable 3-D effects in limiting streamline patterns. Hence, the waviness found in the heat flux distribution could apparently be a demonstration of the existence of steady streaky-like structures (not longitudinal vortices), characterized by stripiness in the streamwise velocity. The near-wall streaks with higher kinetic energy (high-velocity streaks) show higher heat flux levels, and vice versa.

Figure 6 shows heat flux distributions resembling the flow on the flat plate without and with a compression wedge of $\alpha = 25°$ in the presence of the same leading-edge VG strips. The distribution in figure 6(*b*) shows some important flow features typical of separated flows. Those are the incoming flows with low heat flux levels, the separation zone between the meandered separation (S) and reattachment (R) lines, and the flow region downstream of the reattachment region with distinct longitudinal structures.

The leading and trailing edges of the compression wedge are marked by dashed lines (kink-lines K and K').

The traces of streamwise structures visible inside the separation zone and further downstream seem to be clearly linked to the traces observed in the incoming flow upstream of the separation line (figure 6). This suggests that the vortical disturbances generated in the laminar flow by the leading-edge strips induce longitudinal streaky structures, which are enhanced later as longitudinal vortices in the reattachment region of the turbulent ramp flow and become visible in the surface distributions of the main flow parameters. It is also noticeable that the streaky structures identified above as having higher kinetic energy (streaks with higher heat flux levels) cause correspondingly a delay of flow separation, as well as a local decrease in the separation length (see separation S and reattachment R lines, meandering in counter-phase, figure 6*b*). This effect, probably playing a key role in the topology and reappearance of counter-rotating vortices, will be discussed later in more detail.

3.2. *The nature of long-lasting streamwise vortices in fully turbulent flows*

One of the most common features of turbulent flows is the presence of longitudinal streaks with a typical lateral size scaled in wall units of $\lambda_z^+ \approx 100$ characterized by coherent streamwise velocity fluctuations (buffer-layer streaks). These streaks are generated via a self-sustaining closed-loop process, which is initiated by the formation of hairpin vortices. The vortex lift-up effect (e.g. Pujals, Cossu & Depardon 2010) leads to the evidence and amplification of such coherent streaks and finally to the streak's breakdown, enabling the vortex renewal.

Similar elongated coherent structures were revealed recently also in the outer region of the turbulent boundary layers (e.g. Tomkins & Adrian 2003; Ganapathisubramani *et al.* 2006; Hutchins & Marusic 2007). These superstructures exist at typical lateral scales comparable to the boundary-layer thickness δ and are noticeable in large-scale stripiness of the streamwise velocity fluctuations, showing a coherent behaviour for streamwise distances up to 40δ. Moreover, they can contain the biggest part of the turbulent kinetic energy (Pujals *et al.* 2010) and seem to be responsible for large-scale low-frequency streamwise fluctuations (expansion/contraction) of separation zones, etc. (Ganapathisubramani, Clemens & Dolling 2007).

It is commonly assumed that the formation of large-scale streaky structures in turbulent flows results from the agglomeration of a huge number of coherent hairpin vortices, so that these streaks could not exist without the small-scale structures (e.g. Kim & Adrian 1999; Tomkins & Adrian 2003). If the streaky motions at very large scales really are forced by the agglomeration of smaller vortices, that would apparently represent an inverse-energy cascade mechanism, mentioned above.

Nevertheless, some recent results (del Alamo & Jimenez 2006; Kitoh & Umeki 2008; Cossu, Pujals & Depardon 2009; Hwang & Cossu 2010; Pujals *et al.* 2010) show that large-scale streamwise streaks in turbulent channel flows can be amplified directly by the coherent lift-up effect without any procurement of smaller-scale coherent structures. In the experiments (Kitoh & Umeki 2008; Pujals *et al.* 2010), for example, large-scale coherent streaks have been artificially induced via forcing steady large-scale streamwise vortices and, consequently, the mean-flow energy introduced to artificially forced longitudinal vortices has apparently been transferred to the large-scale coherent streaky structures. These outcomes show that the large-scale motions in the turbulent channel flow should not result from small-scale hairpin vortices or buffer-layer streaks.

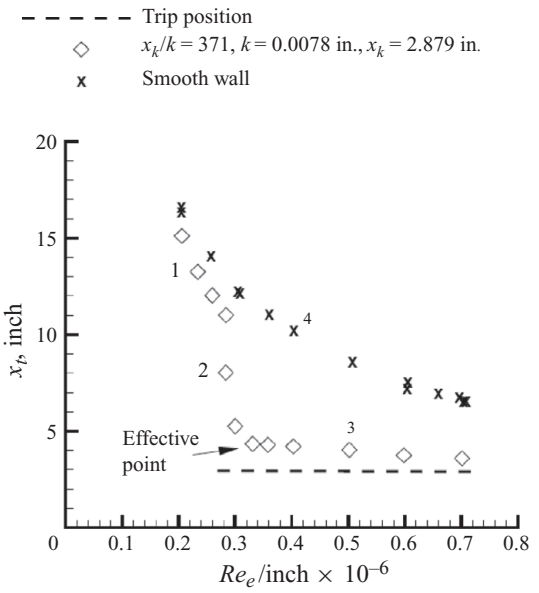

FIGURE 7. Variation of transition location with unit Reynolds number on a 5° half-angle sharp cone at $M_\infty = 2.71$ (results of Van Driest & Blumer 1962 reprinted in Schneider 2007).

As concluded by Hwang & Cossu (2010), the large-scale streaks seem to be a part of self-sustaining processes, which include the formation of large-scale longitudinal vortices, leading to the incidence of coherent large-scale streaks, their downstream amplification accompanied by a sinusoidal oscillation, with final breakdown of streaks. The repetitive regeneration of the longitudinal vortices complete the cycle. While this mechanism exists, the conventional direct-energy-cascade mechanism of energy dissipation can take place.

The typical dimensions of these coherent meandering superstructures closely resemble those of steady longitudinal vortices observed in turbulent ramp flows. It is even likely that the self-sustaining process described is in fact the mechanism supporting the conservation of longitudinal disturbances that we are looking for. So, it can be expected that behind the low-profile vortex generators, the streaky superstructures, which otherwise exist in flat-plate boundary layers as unsteady meandering longitudinal clusters, become steady. This seems plausible, because each model-bonded roughness element or leading-edge discontinuity acts as an anchor for the induced steady longitudinal vortices (see Schülein 2002). Otherwise, as long as the flow is dominated by the non-stationary free-stream disturbances, occurring when the model leading edge and surface are finished sufficiently well and cause no considerable disturbances compared to the free-stream level, the large-scale streaks remain unsteady.

The tripping effect of roughness elements seems to play a very important role here. A detailed recent review of roughness effects on laminar–turbulent transition in high-speed flows can be found in Schneider (2007). As shown there for the results obtained, for instance, by Van Driest & Blumer (1962), the roughness affects the transition location if the roughness size becomes larger than the necessary critical value (figure 7, data 2). The roughness is termed ‘effective’ when it trips the boundary layer as effectively as possible (figure 7, data 3). The difference in the transition

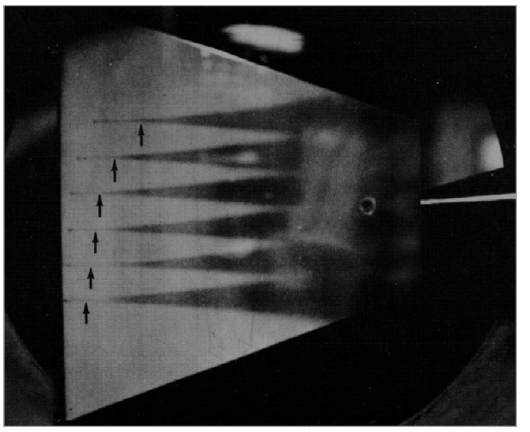

FIGURE 8. Effect of boundary layer tripping by triangular trips (VGs) visualized using fluorene sublimation (results of Hicks & Harper 1970 reprinted in Schneider 2007).

locations for ineffective small roughness (data 1) and for a smooth wall (data 4) is noticeable too, because even at these undersized roughness elements, each of them generates a wake with streamwise vorticity, leading correspondingly to longitudinal streaks, which grow and break down to turbulence with the creation of a turbulent wedge somewhat earlier (see Schneider 2007).

Visualization of the transition caused by isolated triangular roughness elements on a flat plate (Hicks & Harper 1970) is shown in figure 8. The transition to turbulence in the wakes of triangular trips starts at different distances downstream of them (shown by arrows) dependent on the thickness of the boundary layer at the location of each roughness element.

Thus, the idea proposed in the present work is to accent the influence of turbulent wedges or spots, which either exist permanently in the wakes of isolated roughness elements and notches or emerge more stochastically in transitional flows dominated by non-stationary disturbances. The development of turbulent wedges or spots inside of the incoming 2-D laminar flow leads to the local thickening of the boundary layer along its centrelines accompanied by the creation of concave streamline curvature in the outer parts of the boundary layer, leading to the amplification of vortical disturbances. This mechanism may be one of the reasons why these disturbances induced by roughness elements can survive over relatively long distances and become visible as longitudinal vortices in regions with concave streamline curvature in fully turbulent flows.

At perfectly prepared leading edges and surfaces, where the roughness elements or notches are carefully eliminated, the turbulent wedges or spots emerge more stochastically in the flat-plate transition zone. Consequently, the longitudinal superstructures are also not fixed to the model surface and indicate the lateral position of the turbulent spots dominant at present. The low-frequency renewal and replacement of dominant spots apparently lead to the meandering superstructures. If that is correct, then the typical lifetime of dominant spots can be used to determine the longitudinal size of the induced large-scale streaks at known free-stream velocity. The unsteadiness of this process would explain why the footprints of the longitudinal vortices in ramp flows are invisible on models with carefully prepared leading edges. All traditionally used surface-flow visualization techniques, such as the oil-flow method, show only mean-flow limiting streamline patterns.

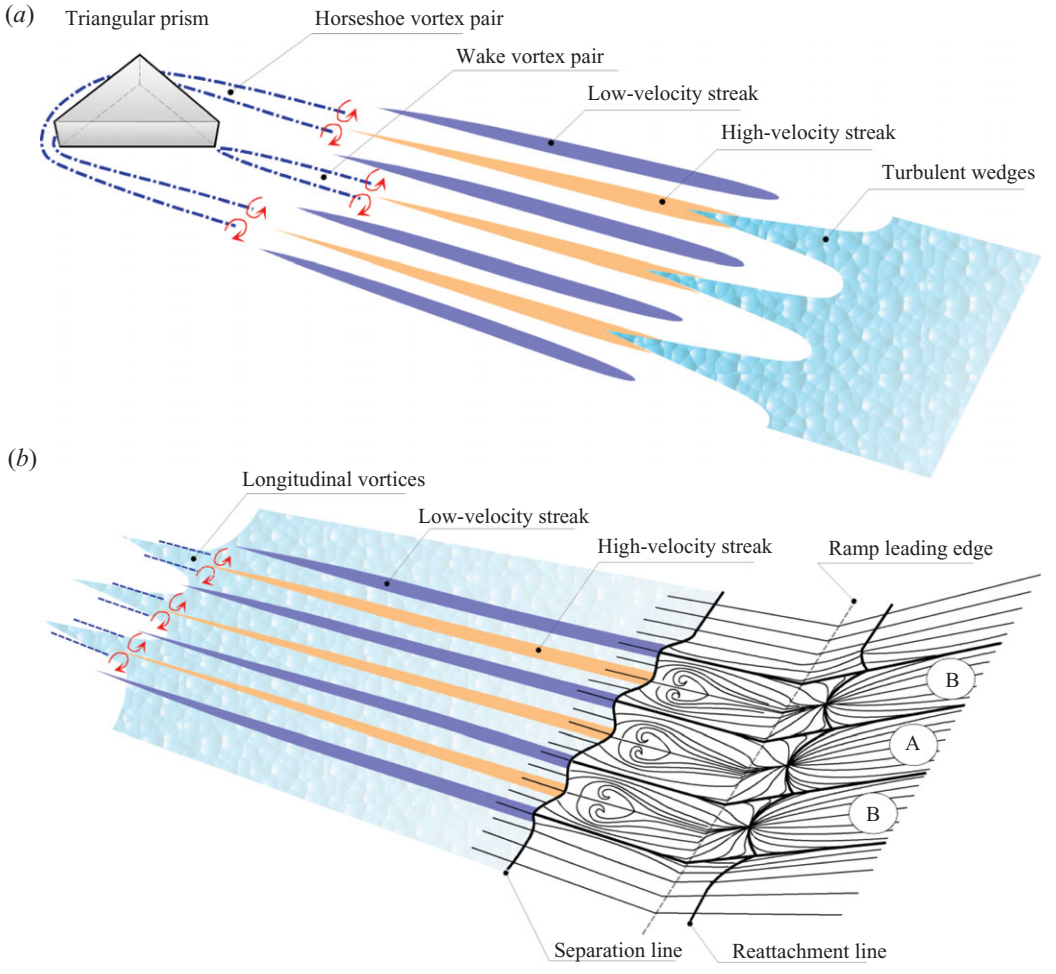

FIGURE 9. Proposed effect of single prism-type vortex generator. (*a*) Estimated effect of longitudinal disturbances, generated by the triangular prism, on the laminar–turbulent transition. (*b*) Further development of the vortical disturbances, leading to the formation of longitudinal vortices near the separation region.

3.3. *Influence of the relative size of a single LPVG on the downstream flow topology*

The vortical structure in the presence of a triangular-prism VG and its assumed effect on the flow topology generated far downstream near the ramp are sketched in figure 9. Figure 9(*a*) demonstrates the estimated effect of longitudinal disturbances, generated by the triangular prism, on the laminar–turbulent transition process via generation, growth and breakdown of steady streamwise streaks in the laminar boundary layer with formation of turbulent wedges.

In the next stage of the flow development (figure 9*b*), the existing vortical disturbances start a new self-sustaining process in the turbulent boundary layer, which is accompanied by formation and amplification of steady streaky superstructures, leading finally to the reappearance of longitudinal vortices in the ramp flow. In some sense, each vortex pair induced near the reattachment region on the ramp is a child of a vortex pair, which was generated originally by the VG or by the roughness element near the leading edge.

Two types of vortex pairs, which could be forced artificially by the low-profile VGs, were identified in the supersonic turbulent separated flows: the A- and the B-type vortex pairs (figure 9). The investigations show that the A-type vortices are induced by the longitudinal vortices initially generated in the wake region of the VG due to the interaction of the wake flow with the recompression shock waves. The B-type vortex pairs emerge when the conditions for a distinct horseshoe separation at the face of the leading-edge VG occur. As shown in the sketches, a relatively wide and high triangular-prism VG typically induced three vortex pairs: one A- and two B-type vortex pairs.

It is important to note that the steady low-momentum streaks in the incoming boundary layer cause an earlier flow separation as well as a later reattachment, while the high-momentum streaks, in contrast, delay the separation. A similar effect is shown to cause the large-scale low-frequency unsteadiness (repetitive extraction and contraction) of the shock-induced separation regions (see Ganapathisubramani *et al.* 2007) due to existence of unsteady streaky low- and high-momentum superstructures in the upstream turbulent boundary layer.

The influence of the streamwise-streak amplitude on the limiting streamline pattern on the ramp is presented in figure 10, showing an interpretation of the oil-flow visualizations obtained in experiments at different thicknesses h_g and distances x_s of an LPVG. The increase of the disturbance amplitude (see sketches from top to bottom) causes the appearance of an 'oil-face' structure, proposed for three-dimensional (3-D) steady separated flows by Hornung & Perry (1982) (see also Hornung 1983; Bippes & Turk 1984). This flow structure is characterized at the beginning by the formation of a secondary separation bubble with a pair of focus points (node points N_3 and N_4) inside the separation bubble. At further increase of the momentum difference in the low- and high-velocity streaks (high VG at shortest investigated distances x_s), the flow energized by the high-velocity streak apparently penetrates deep into the zone of adverse pressure gradient, causing the change in the flow topology. In this case, the limiting streamline pattern classified by Hornung & Perry (1982) as an oil-face of the fourth kind occurs.

The influence of the relative size of a single prism VG on the flow topology generated downstream near the ramp has been investigated by varying the dimensionless generator's height h_g/δ_g and span a_g/λ, as well as the distance x_g/δ_g. The base shape of the prism VG used was an equilateral triangle. Skin-friction line visualizations show that the vortex generator sizes have a distinct influence on the flow topology near the ramp.

In addition to the most common combination of A and B vortex structures presented in figure 9, some other special cases for smaller VGs can be defined. At a *high* VG, the flow near the top leading edge at $y = h_g$ is supersonic and two very intense horseshoe vortex pairs appear in the reattachment region of the ramp flow, while at a subsonic leading edge (*low-height* VG), these footprints could not be observed. For the Mach 3 case, the sonic line at $x_g = 5\,\text{mm}$ is located at a wall-normal distance of $y = 0.08\,\text{mm}$, and for Mach 5 at $y = 0.05\,\text{mm}$.

The lateral size a_g of the VG is best represented in terms of the typical diameter of the induced vortex pairs λ. Hence, $a_g \geqslant 3\lambda$ corresponds to a *wide* VG, while $a_g < 3\lambda$ indicates a *low-span* case. The first case (wide VG) is characterized by the footprints of the A-type vortex pair in the resulting ramp flow, while at the low-span VG, in contrast, the limiting streamline pattern indicates absence of this vortex pair. If the spacing between the induced vortex pairs is not big enough, the B-type vortices are found to be dominant in the resulting flows.

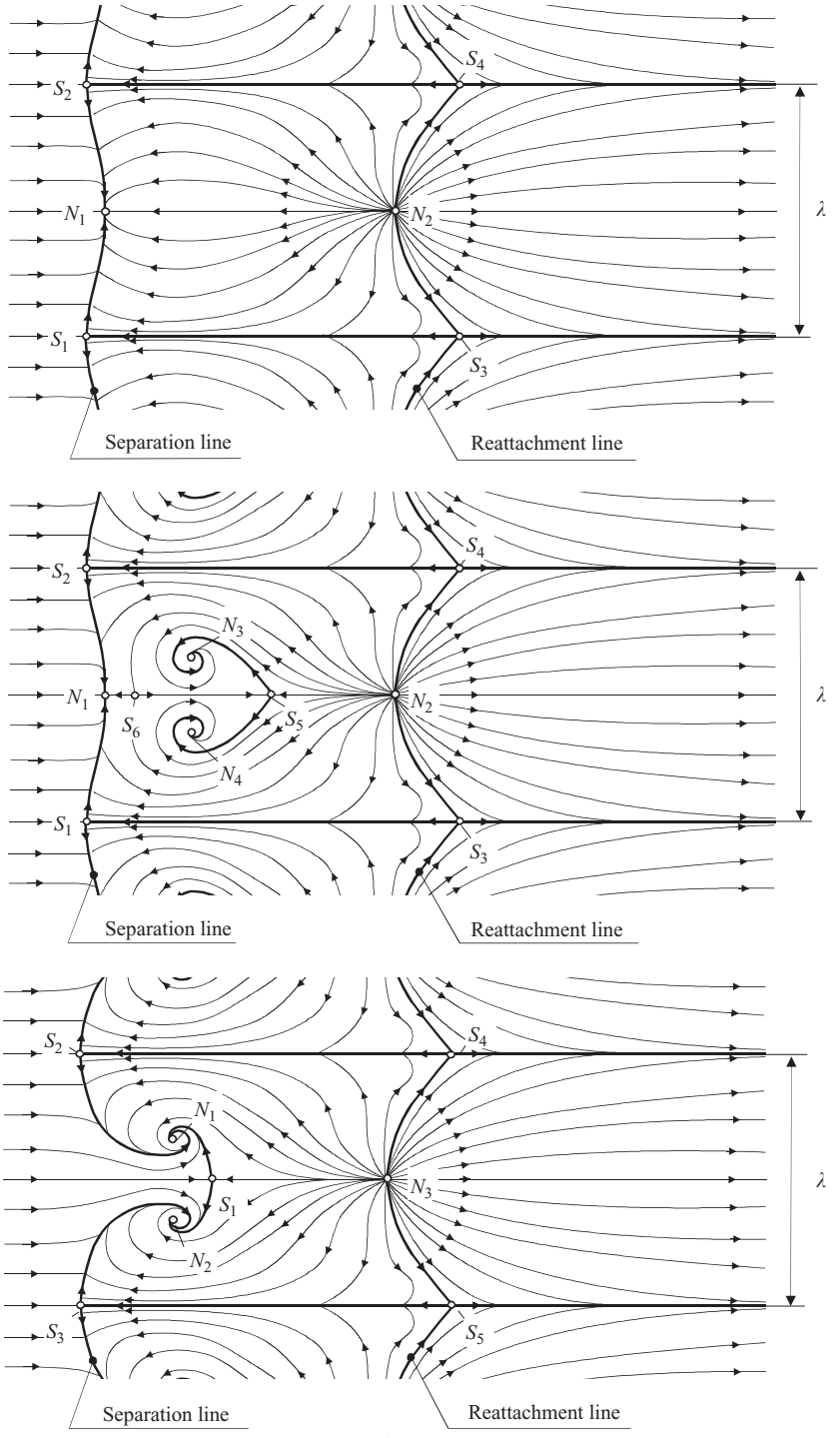

FIGURE 10. Interpretation of the skin-friction pattern in the separation region of the ramp flow obtained experimentally. The sketches presented correspond to, from top to bottom, streaky disturbances of increasing amplitude in the upstream boundary layer. This effect was achieved in the experiments by variation of the parameters h_g and x_s: higher h_g and shorter x_s cause more intense disturbances.

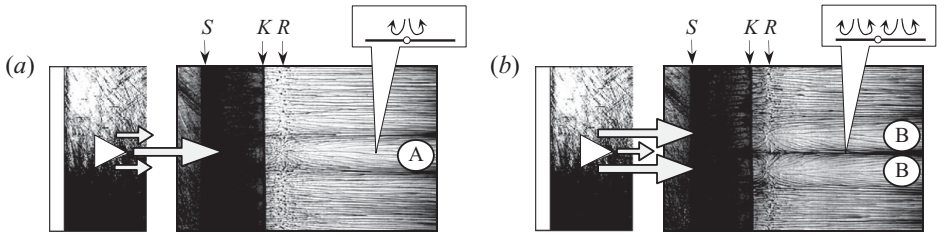

FIGURE 11. Left side: leading edge of the plate (single triangular-prism VG, $x_g = 5\,\text{mm}$, $a_g = 5\,\text{mm}$). Right side: oil-flow pattern on the 2-D compression corner $\alpha = 20^\circ$ ($M_\infty = 3$, $Re_1 = 26 \times 10^6\ \text{m}^{-1}$) at $x_s = 390\,\text{mm}$, (*a*) $h_g = 0.05\,\text{mm}$, (*b*) $h_g = 0.2\,\text{mm}$. *S* and *R* denote the ramp-flow separation and reattachment lines; *K* shows the position of the ramp's leading-edge kink.

Two different vortex topologies in the ramp flow, demonstrating this behaviour, have been observed in the experiments presented in figure 11. For a low-height vortex generator ($h_g = 0.05\,\text{mm}$ at $x_g = 5\,\text{mm}$, figure 11*a*), the results demonstrate the footprint of a pair of streamwise vortices (A-type) with a longitudinal divergence line shedding from the rear corner of the triangular generator. Note that the negatives of oil-flow visualizations are shown. The footprint of the vortex pair is embedded between two longitudinal convergence lines. The dominant and suppressed vortex pairs are illustrated in figure 11 by bigger and smaller arrows, respectively. The scale used is only of qualitative character and not a measure of absolute vortex pair strength. The increase in the generator's height h_g up to 0.2 mm (figure 11*b*) yielded another type of flow structure on the ramp with two pairs of streamwise vortices (B-type). A downstream displacement of this higher vortex generator ($h_g = 0.2\,\text{mm}$) to the location $x_g = 75\,\text{mm}$ with a thicker local boundary layer δ_g transfers the vortex structure again to that shown in figure 11(*a*). These experiments demonstrate the existence of a critical value for the ratio h_g/δ_g for a single VG. The vortex structure induced in the ramp flow changes within a narrow range of h_g/δ_g, but not abruptly.

Of course, the value h_g/δ_g alone cannot be a general criterion for prediction of vortex topology generated by the LPVG at different flow conditions. The dimensionless size of roughness elements $h_g^+ = u_\tau h_g/\nu$, including the relation of the friction velocity u_τ to the kinematic viscosity ν, well known from boundary layer theory, could be a more general parameter. The analysis of the present data shows that the transition between the two different vortex structures occurs at values of h_g^+ between 10 and 20. Another well-accepted correlation parameter for studying the effects of roughness on transition is the roughness Reynolds number defined as $Re_k = U_k k/\nu_k$, where k is the roughness size, while U_k and ν_k denote the velocity and viscosity of the flow at the edge of the roughness element (see Schneider 2007). In the nomenclature of the present work, Re_k corresponds to $Re_g = U_g h_g/\nu_g$. The most important difference between Re_g and h_g^+ is obviously the use of U_g instead of u_τ. Which of these two parameters is more suitable as correlation parameter requires further investigation.

3.4. *Natural scale of longitudinal vortex pairs*

The experimental investigation of the generator's wavelength λ_g effect by Schülein (2002) clearly showed that the generated vortex pairs have always retained a certain common wavelength and are not freely scalable for fixed flow conditions. For λ_g essentially bigger than λ, the gap between neighbouring vortex pairs was filled with nearly 2-D flow or with additional weaker vortices. If λ_g was essentially smaller than λ,

all vortex footprints practically vanish from the oil-flow pattern. For given conditions, the value of λ could be determined by Schülein (2002) approximately between 4.9 and 5.7 mm. This value of the VG spacing corresponds to twice the diameter of the dominant longitudinal vortices and was approximately equal to the incoming boundary-layer thickness δ_1 or somewhat bigger. A lower limit for the ratio λ_g/δ_1 of approximately 0.8–0.9 was identified by Schülein (2002), below which no vortex could be generated artificially. Note that the cited investigations were performed for constant ramp location on the plate and thus constant boundary layer thickness δ_1. Consequently, the cited relative distance λ_g/δ_1 has no general validity and should be clarified by variation of the boundary-layer thickness.

The numerical investigations by Lüdeke (2003) confirmed that for a series of investigated wavelengths λ_g (3, 6, 9 and 12 mm), the generated vortex pairs become most intense for a generator wavelength $\lambda_g = 6$ mm. For smaller and bigger wavelengths, the vortex effects at the reattachment areas of the ramps weaken, and the natural scales λ of vortex pairs could not be derived from these results.

A list of parameters, which may have an influence on the lateral dimensions of longitudinal vortices in the reattachment region of a compression wedge located at a distance Δx_g from the trailing edge of the VG, can be compiled based on obtained and available data of streamwise structures. The natural scale or wavelength λ of a longitudinal vortex pair depends, in general, on the local boundary-layer thickness and on a set of external factors:

$$\frac{\lambda}{\delta_1} = f\left(M_\infty, Re_\infty, \alpha, \frac{\Delta x_g}{\delta_g}, \frac{h_g}{\delta_g}, \frac{a_g}{\delta_1}, \frac{\lambda_g}{\delta_1}, \frac{p_2}{p_1}, \Delta c_p, \frac{T_g}{T_0}, VGT\right). \tag{3.1}$$

Here, λ_g is the generator-to-generator spacing, h_g is the height of the vortex generator, δ_g and δ_1 are the boundary-layer thicknesses at the generator's and ramp's location for the undisturbed flat-plate boundary layer, p_2/p_1 is the shock strength, $\Delta c_p = c_{p2} - c_{p1}$ is the dimensionless pressure jump due to the shock wave, α is the deflection angle of the ramp, T_g/T_0 is the ratio of the generator's temperature to the total temperature, VGT is the type or configuration of vortex generator used, and x_g is the distance between the VG's and the plate's leading edges.

3.5. *Effect of the boundary-layer thickness at the shock position*

The dependence of the wavelength on the boundary-layer thickness had been assumed since the discovery of the longitudinal structures. However, the known approximations were not systematic and did not take into account all relevant parameters. That is why in the present investigations no comparisons with other data have been carried out.

The new results obtained in the present work confirm the described statements and show that the local thickness of the boundary layer is one of the most important scaling parameters. In fact, depending on the introduced wavelength λ_g of the periodic generators, three topologically different flow patterns in the shock wave/boundary layer interaction region can be observed: a two-dimensional flow without generated vortices, flow with narrowly packed streamwise structures or a pattern that reveals the natural scale λ of the streamwise structures on the background of a quasi-two-dimensional flow. The last flow pattern allows the evaluation of the natural scales of the longitudinal vortices.

Figure 12(a–j) shows on the right-hand side distinct footprints of longitudinal structures on the 25° compression wedge installed at different distances x_s($x_s = \Delta x_g + x_g$). The photos to the left show the vortex generators used, respectively, at the plate's

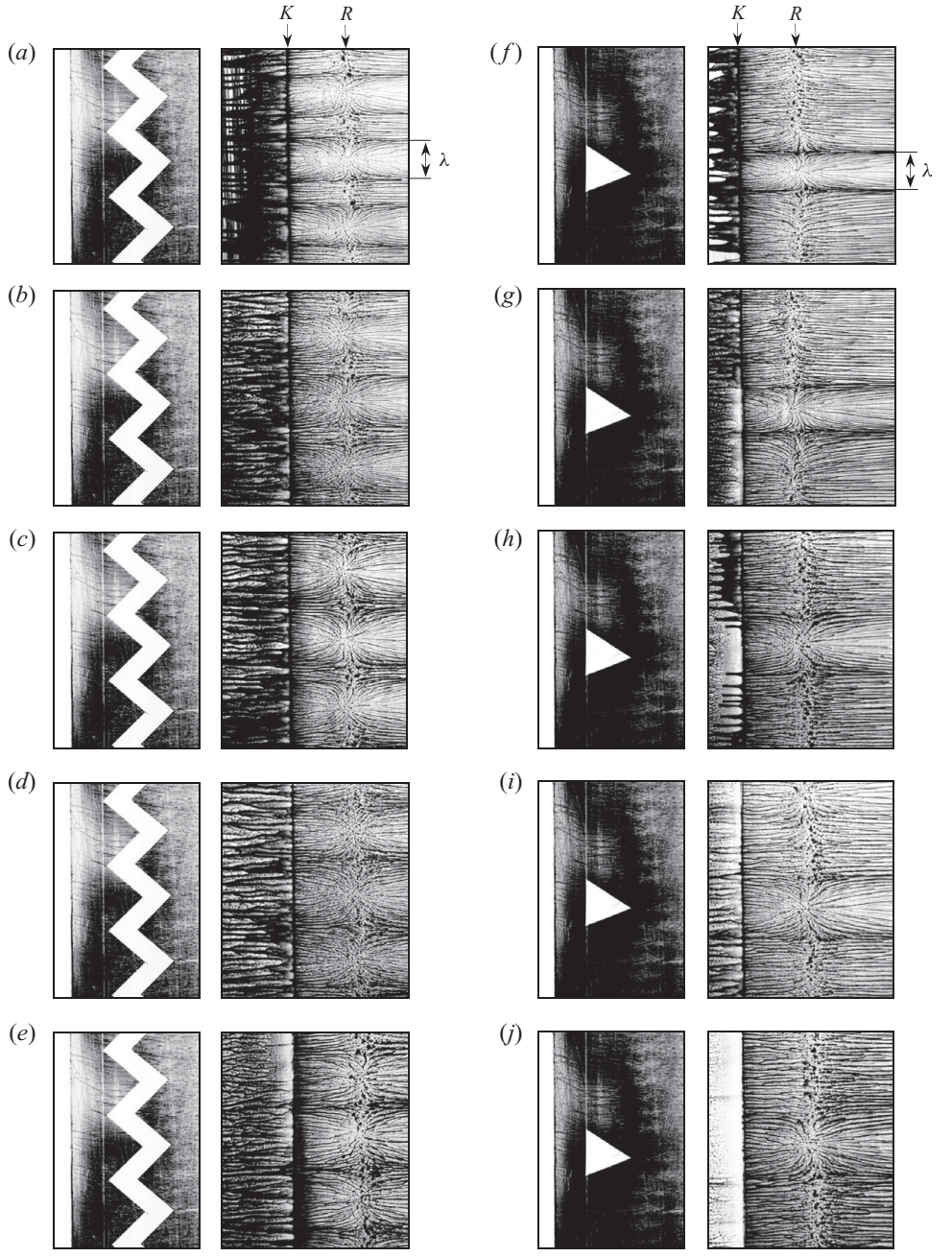

FIGURE 12. Left side: (*a–e*) photos of the strip VG used ($\lambda_g = 11.3$ mm, $h_g = 0.05$ mm, $x_g = 5$ mm); (*f–j*) photos of the triangular-prism VG used ($a_g = 7$ mm, $h_g = 0.05$ mm, $x_g = 5$ mm). Right side: (*a–j*) oil-flow pictures on the 2-D compression corner $\alpha = 25°$ ($M_\infty = 3$, $Re_1 = 30 \times 10^6$ m^{-1}) at different distances x_s, (*a*) 225 mm, (*b*) 275 mm, (*c*) 325 mm, (*d*) 375 mm, (*e*) 475 mm, (*f*) 225 mm, (*g*) 275 mm, (*h*) 325 mm, (*i*) 375 mm, (*j*) 475 mm. *S* and *R* denote the ramp-flow separation and reattachment lines; *K* shows the position of the model kink.

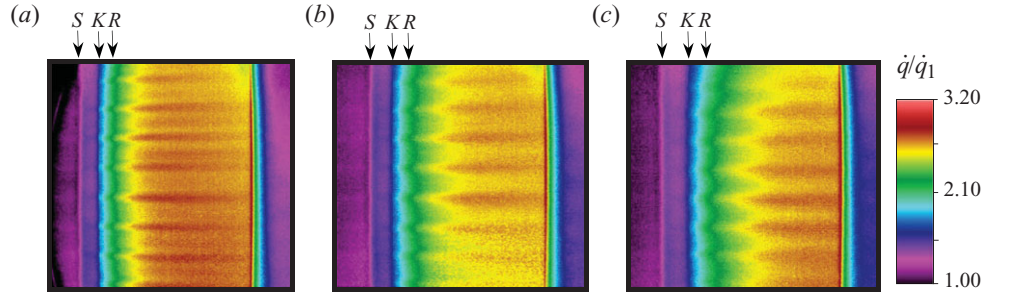

FIGURE 13. Heat flux ratio distribution on the compression corner of $\alpha = 20°$ at $M_\infty = 3$ with LPVG ($h_g = 0.05$ mm, $\lambda_g = 11.3$ mm): (*a*) $Re_x = 5.85 \times 10^6$ ($x_s = 225$ mm) with $\dot{q}_1 = 4440$ W m^{-2}; (*b*) $Re_x = 8.45 \times 10^6$ ($x_s = 325$ mm) with $\dot{q}_1 = 4170$ W m^{-2}; (*c*) $Re_x = 11.05 \times 10^6$ ($x_s = 425$ mm) with $\dot{q}_1 = 3990$ W m^{-2}. *S* and *R* denote the ramp-flow separation and reattachment lines; *K* shows the position of the model kink.

leading edge. All oil-flow visualizations shown, especially at smallest distances x_s (see figure 12*a*,*f*), display the existence of natural scales λ for the generated streamwise vortices. The streamlines indicate distinct footprints of vortex pairs separated by regions with nearly quasi-parallel flow in between. It is remarkable that the lateral vortex spacing λ is dependent only on the distance x_s and not on the VG type (figure 12*a*–*e*, periodic strip VG; figure 12*f*–*j*, triangular-prism VG). It can definitely be seen that in all these cases, the wavelength of the vortex pairs increases with the distance x_s and correspondingly with the local thickness of the boundary layer δ_1 upstream of the compression wedge.

This effect was also confirmed by the results of heat flux measurements for different wedge locations downstream of the low-profile VG. Figure 13 shows the normalized distributions of heat flux rates at three different $x_s = 225$, 325 and 425 mm. These tests with periodic generators of $h_g = 0.05$ mm and $\lambda_g = 11.3$ mm and the compression wedge of 20° revealed distinct longitudinal structures. The heat flux patterns (figure 13*a*), indicating longitudinal streaks with higher heat flux levels (single vortex pairs) and the gaps between them, are similar to the observed oil-flow visualization pictures. At larger distances x_s, the transverse size λ of each vortex-pair footprint becomes larger.

Figure 14 shows a detailed interpretation of the experimentally obtained limiting-streamline pattern, characterizing the footprint of a longitudinal vortex pair when the λ_g is bigger than the vortex pair diameter. In this case, the gap between neighbouring vortex pairs can clearly be seen, allowing the determination of λ.

3.6. *Effect of the compression corner angle*

The effect of the compression angle on the intensity and transverse size of streamwise structures is illustrated in figure 15 for the compression angles of 20°, 25° and 30°, respectively. The properties of surface heat flux distributions agree fairly well with oil-flow visualization data. Most distinct is the extension of the separation region near the compression wedge and the increase in the intensity and scale of the streamwise structures with increasing compression angle.

The dependencies of the obtained natural wavelengths λ on the distance x_s and on the local boundary-layer thickness δ_1 for moderate compression angles of $\alpha = 20°$ and 25° are shown in figures 16 and 17. The values for δ_1 at investigated x_s-distances were calculated by simplified empirical correlations, which are proposed by Chappel

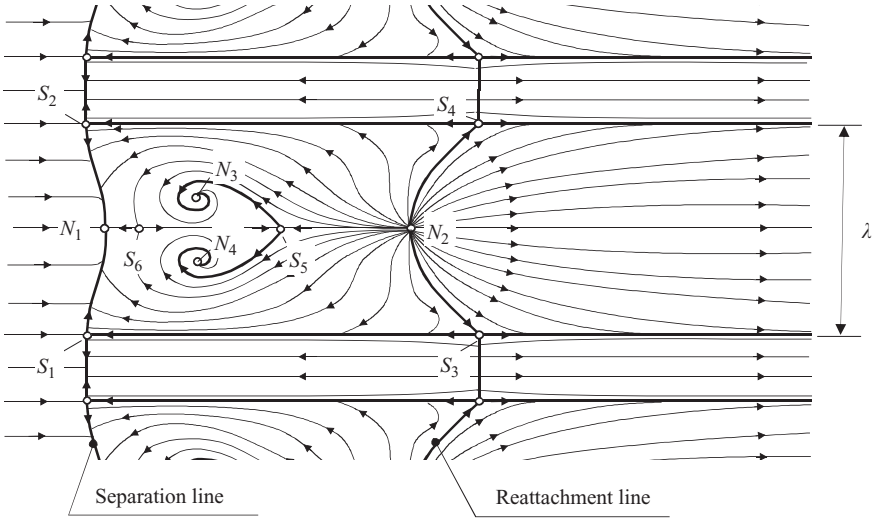

FIGURE 14. Sketch of the skin-friction pattern in the separation zone region of the ramp flow downstream of a zigzag-strip VG for the case $\lambda_g > \lambda$.

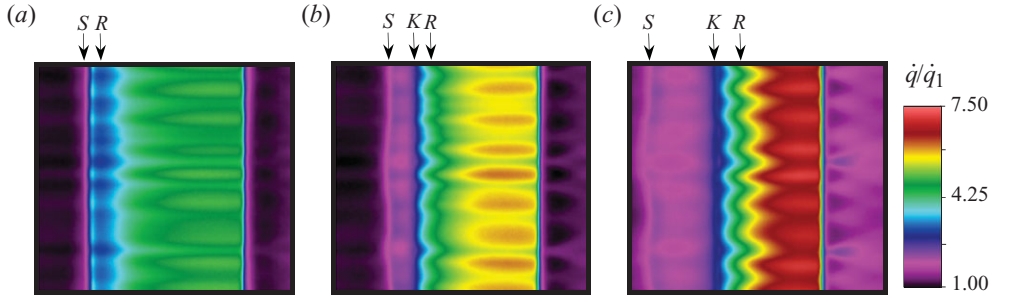

FIGURE 15. Heat flux ratio distribution on compression corner at $M_\infty = 5$ and $Re_x = 19.5 \times 10^6$ with a strip-LPVG ($x_g = 5$ mm, $h_g = 0.2$ mm, $\lambda_g = 11.3$ mm) at different α with $\dot{q}_1 = 11\,800$ W m^{-2}: (*a*) $\alpha = 20°$; (*b*) $\alpha = 25°$; (*c*) $\alpha = 30°$. *S* and *R* denote the ramp-flow separation and reattachment lines; *K* shows the position of the model kink.

(1970) for turbulent flows. The agreement of the values that were obtained with single triangular-prism VGs and with zigzag-strip VGs at $\alpha = 25°$ is remarkable.

The effect of the compression angle α on the wavelength λ turned out to be most pronounced, as shown in figure 16. The obvious increase of the wavelength λ with the change of the compression angle α from 20° to 25° is significant. The very strong dependence shows that the boundary-layer thickness is responsible for the wavelength scaling. Moreover, the increase of the vortex wavelength with the thickness of the boundary layer for a wedge angle of 25° is approximately twice as high as in the case of $\alpha = 20°$. Consequently, the relation of the wavelength to the boundary-layer thickness λ/δ_1 depends on the compression angle α (figure 17).

How does the compression angle influence the transverse size of streamwise structures? As shown above, the initial disturbances from the LPVG, which is located near the leading edge, remain weak up to the compression-wedge location and subsequently amplify in the reattachment zone with formation of intense longitudinal vortical structures. With increase of the compression angle, the size of the separation

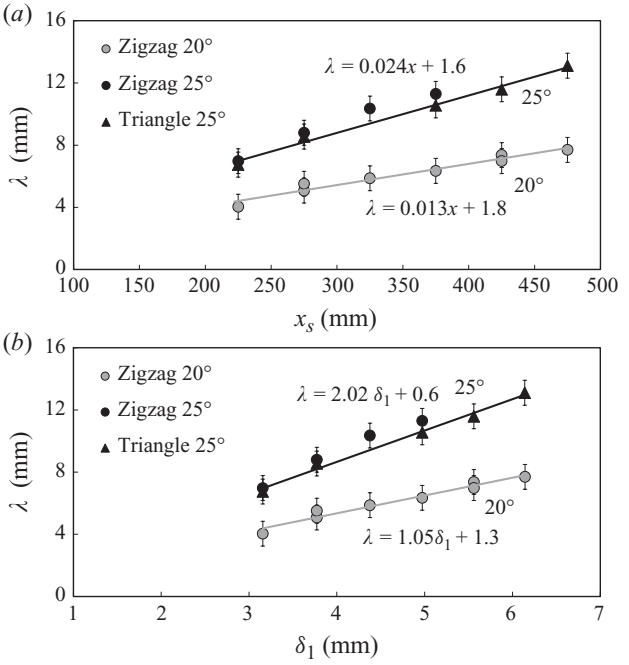

FIGURE 16. Effect of compression angle and boundary-layer thickness at $M_\infty = 3$: (*a*) λ versus x_s; (*b*) λ versus δ_1.

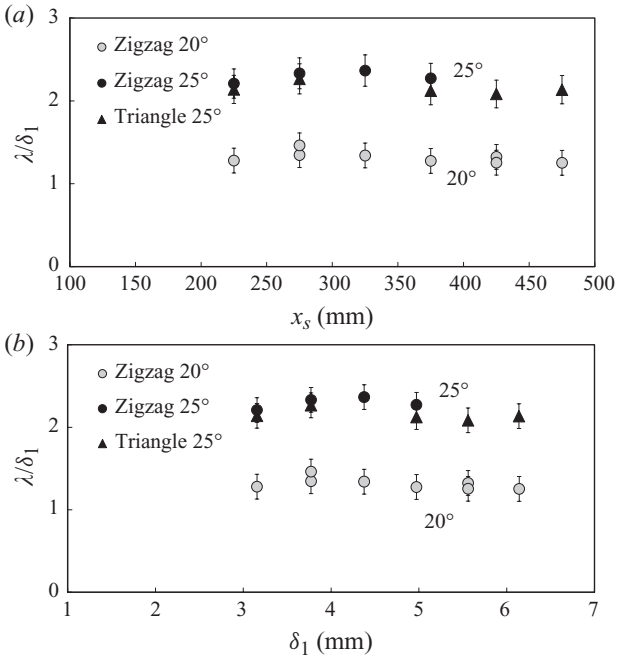

FIGURE 17. Effect of compression angle and boundary-layer thickness at $M_\infty = 3$: (*a*) λ/δ_1 versus x_s; (*b*) λ/δ_1 versus δ_1.

zone increases as well as the streamwise pressure gradient and the pressure jump Δc_p. Both parameters amplify the generator-induced disturbance, and an increase in the vortex intensity and in the streamwise scale of the structures can be expected.

4. Conclusions

The most important results of the study can be summarized as follows.

(i) The longitudinal vortical disturbances, which are initiated by leading edge or surface irregularities that represent hydraulic roughness, survive over very large downstream distances within the fully developed turbulent flow. The present investigations have shown that such streamwise vortical disturbances exist in turbulent supersonic flows on flat plates without pressure gradients over distances of the order of 10^4 vortex-generator heights. The interaction of the boundary layer with strong adverse pressure gradients accompanied by flow separation leads to the amplification of these disturbances and to the development of intense longitudinal vortex pairs in the reattachment region.

(ii) The total number, dimension and type of installed vortex generators define the number of vortex pairs generated downstream. In some sense, each vortex pair induced near the reattachment region on the ramp is a child of a vortex pair, which was generated originally by the VG or by the roughness element near the leading edge.

(iii) Two types of vortex pairs in turbulent separated flows, which could be forced artificially by single leading-edge LPVGs, were identified: the A- and the B-type vortex pairs. The A-type vortices are related to the longitudinal vortices generated in the wake region of the VG, while the B-type ones emerge when the conditions for a distinct horseshoe separation upstream of the VG occur. If the spacing between the vortex pairs induced in resulting flows is not large enough, the B-type vortices were found to be dominant.

(iv) It was found that the relative size of the VG has a critical influence on the resulting flow topology. If exceeding the ratio h_g/δ_g, the resulting flow on the turbulent ramp changes the flow structure. Hence, the resulting vortical structure induced, for example, by single triangular prisms in the turbulent ramp flow is different for *high and wide*, *high low-span* and *low-height* vortex generators.

(v) It is proposed that the elongated coherent superstructures, existing in undisturbed turbulent boundary layers as meandering unsteady longitudinal clusters, become steady in tripped turbulent flows. The generation and long-term preservation of vortical disturbances in turbulent flows is triggered by turbulent wedges, existing in the wakes of isolated roughness elements or notches. In the authors' opinion, the vortical disturbances start downstream of the transition region the known self-sustaining process, which is accompanied by formation and amplification of steady streaky superstructures, leading finally to the reappearance of longitudinal vortices in the ramp flow. The quasi-steady longitudinal vortices observed in ramp flows seems to be an indicator for the steadiness of these low- and high-momentum streaks in tripped turbulent boundary layers.

(vi) The transverse sizes of the induced vortices demonstrate certain natural scales (or wavelength) λ typical for local flow conditions. The local thickness parameters δ and δ^* of the turbulent boundary or shear layer are the most important scaling parameters for the characterization of natural scales for the vortex pairs induced.

(vii) The relative wavelength λ/δ_1 remains approximately constant for different distances from the model's leading edge x_s and local boundary-layer thickness δ_1, but

increases with an increasing compression angle, shock wave intensity or separation length.

(viii) The present study yields clear recommendations that allow elimination of steady large-scale longitudinal vortices by means of periodic vortex generators. In order to avoid its footprints on surfaces of wind tunnel models, for example, periodic leading-edge vortex generators (rows of dots or zigzag strips) should be chosen with a wavelength that is noticeably smaller than the boundary-layer thickness at the investigated location ($\lambda_g < 0.7 - 0.8\delta_1$).

REFERENCES

del Alamo, J. C. & Jimenez, J. 2006 Linear energy amplification in turbulent channels. *J. Fluid Mech.* **559**, 205–213.

Berezin, Y. A., Hutter, K. & Zhukov, V. P. 1991 Large-scale vortical structure supported by small-scale turbulent motions: helicity as a cause for inverse energy cascade. *Contin. Mech. Thermodyn.* **3**, 127–146.

Berezin, Y. A. & Trofimov, V. M. 1996 Large-scale vortex generation driven by non-equilibrium turbulence. *Fluid Dyn.* **31** (1), 39–46.

Bippes, H. & Turk, M. 1984 Oil flow patterns of separated flow on a hemisphere cylinder at incidence. *Tech. Rep.* DFVLR-FB 84-20, DFVLR (DLR) Göttingen.

Brazhko, V. 1979 Periodic structure of the flow and heat transfer in the reattachment region of supersonic flow (in Russian). *Uchenye Zapiski TsAGI* **10** (2), 113–118.

Chappel, P. D. 1970 Some correlations for the turbulent boundary layer on a flat plate. *J. R. Aero. Soc.* **74**, 393–396.

Cossu, C., Pujals, G. & Depardon, S. 2009 Optimal transient growth and very large-scale structures in turbulent boundary layers. *J. Fluid Mech.* **619**, 79–94.

Domröse, U., Krause, E. & Meinke, M. 1996 Numerical simulation of laminar hypersonic shock-boundary layer interaction. *Z. Flugwiss. Weltraumforsch.* **20**, 89–94.

Falkovich, G. & Sreenivasan, K. R. 2006 Lessons from hydrodynamic turbulence. *Phys. Today* **59** (4), 43–49.

Ganapathisubramani, B., Clemens, N. T. & Dolling, D. S. 2006 Large-scale motions in a supersonic turbulent boundary layer. *J. Fluid Mech.* **556**, 271–282.

Ganapathisubramani, B., Clemens, N. T. & Dolling, D. S. 2007 Effects of upstream boundary layer on the unsteadiness of shock-induced separation. *J. Fluid Mech.* **585**, 369–394.

Ginoux, J. J. 1958 Experimental evidence of three-dimensional perturbations in the reattachment of a two-dimensional laminar boundary layer at $M = 2.05$. *Tech. Rep.* TCEA TN1, Training Center for Experimental Aerodynamics, Rhode-Saint-Genèse, Belgium.

Ginoux, J. J. 1960 Laminar separation in supersonic flow with emphasis on three-dimensional perturbations at reattachment. *Tech. Rep.* TCEA TN3, Training Center for Experimental Aerodynamics, Rhode-Saint-Genèse, Belgium.

Ginoux, J. J. 1969 On some properties of reattaching laminar and transitional high speed flows. *Tech. Rep.* VKI TN 53, VKI, Rhode-Saint-Genèse, Belgium.

Ginoux, J. J. 1971 Streamwise vortices in reattaching high-speed flows: a suggested approach. *AIAA J.* **9** (4), 759–760.

Görtler, H. 1940 Über eine dreidimensionale Instabilität laminarer Grenzschichten an konkaven Wänden: Nachrichten der Gesellschaft der Wissenschaften zu Göttingen (in German). *Mathematisch-Physikalische Klasse*, **1** (2), pp. 1–26.

Görtler, H. 1941 Instabilität laminarer Grenzschichten an konkaven Wänden gegenüber gewissen dreidimensionalen Störungen. *ZAMM* **21** (4), 250–252.

Henckels, A., Kreins, A. F. & Maurer, F. 1993 Experimental investigations of hypersonic shock-boundary layer interaction. *Z. Flugwiss. Weltraumforsch.* **17**, 116–124.

Hicks, R. M. & Harper, W. R. 1970 A comparison of spherical and triangular boundary-layer trips on a flat plate at supersonic speeds. *Tech. Rep.* TM-X-2146, NASA.

Hornung, H. 1983 The vortex skeleton model for three dimensional steady flows. *Tech. Rep.* AGARD-CP-342, pp. 2-1–2-12.

Hornung, H. & Perry, A. E. 1982 Streamsurface bifurcation, vortex skeletons and separation *Tech. Rep.* DLR IB 222-82 A 25, DFVLR (DLR) Göttingen.

Hutchins, N. & Marusic, I. 2007 Evidence of very long meandering features in the logarithmic region of turbulent boundary layers. *J. Fluid Mech.* **579**, 1–28.

Hwang, Y. & Cossu, C. 2010a Amplification of coherent streaks in the turbulent Couette flow: an input–output analysis at low Reynolds number. *J. Fluid Mech.* **643**, 333–348.

Hwang, Y. & Cossu, C. 2010b Self-sustained process at large scales in turbulent channel flow. *Phys. Rev. Lett.* **105**, 044505.

Kim, K. C. & Adrian, R. J. 1999 Very large-scale motion in the outer layer. *Phys. Fluids* **11**, 417.

Kitoh, O. & Umeki, M. 2008 Experimental study on large-scale streak structure in the core region of turbulent plane Couette flow. *Phys. Fluids* **20**, 025107.

Kraichnan, R. H. 1973 Helical turbulence and absolute equilibrium. *J. Fluid Mech.* **59**, 745–752.

Kreins, A. F., Henckels, A. & Maurer, F. 1996 Experimental studies of hypersonic shock induced boundary layer separation. *Z. Flugwiss. Weltraumforsch.* **20**, 80–88.

Lin, J. C. 2002 Review of research on low-profile vortex generators to control boundary-layer separation. *Prog. Aerosp. Sci.* **38**, 389–420.

Lüdeke, H. 2003 Untersuchungen von Längswirbeln in abgelösten hypersonischen Strömungen (in German). *Tech. Rep.* DLR FB 2003-04, DLR Braunschweig.

Lüdeke, H., Radespiel, R. & Schülein, E. 2004 Simulation of streamwise vortices at the flaps of re-entry vehicles. In *AIAA 2004-0915*, 42*nd AIAA Aerospace Sciences Meeting and Exhibit*, Reno, NV.

Lüdeke, H. & Schülein, E. 2002 Simulation of streamwise vortices on turbulent hypersonic ramps. In *Proceedings of the Second International Conference on CFD*, University of Sydney, Australia.

Marusic, I., McKeon, B. J., Monkewitz, P. A., Nagib, H. M., Smits, A. J. & Sreenivasan, K. R. 2010 Wall-bounded turbulent flows at high Reynolds numbers: recent advances and key issues. *Phys. Fluids* **22** 065103.

Maurer, E. 1966 Three-dimensional effects in shock-separated flow regions ahead of lateral control-jets issuing from slot nozzles of finite length. *Tech. Rep.* AGARD-CP-4, Separated Flows, part 2, pp. 605–634.

Moiseev, S. S., Sagdeev, R. Z., Tur, A. V. & Yanovsky, V. V. 1983 Theory of formation of large-scale structures in hydro-dynamical turbulence (in Russian). *J. Exp. Theor. Phys.* **85**, 1979–1987.

Pearcey, H. H. 1961 Shock induced separation and its prevention by design and boundary layer control. In *Boundary Layer and Flow Control* (ed. G. V. Lachmann). vol. 2, pp. 1277–1312. Pergamon.

Pujals, G., Cossu, C. & Depardon, S. 2010 Forcing large-scale coherent streaks in zero pressure gradient turbulent boundary layer. *J. Turbul.* **11**, 25.

Roshko, A. & Thomke, G. J. 1966 Observations of turbulent reattachment behind an axisymmetric downstream-facing step in supersonic flow. *AIAA J.* **4** (6), 975–980.

Schneider, S. P. 2007 Effects of roughness on hypersonic boundary-layer transition. In *AIAA*-2007-305, 45*th* AIAA Aerospace Sciences Meeting and Exhibit, Reno, NV.

Schülein, E. 1999 Qualität der Strömung nach der Nachbearbeitung der Überschalldüse '$M = 3$' des Rohrwindkanals des DLR in Göttingen (in German). *Tech. Rep.* DLR IB 223-99 A 12, DLR Göttingen.

Schülein, E. 2002 Experimentelle Untersuchungen zur Längswirbelbildung in turbulenten Überschallströmungen mit Ablösungen (in German). *Tech. Rep.* DLR IB 224-02 A 12, DLR Göttingen.

Schülein, E. 2006 Skin friction and heat flux measurements in shock boundary layer interaction flows. *AIAA J.* **44** (8), 1732–1741.

Schülein, E., Krogmann, P. & Stanewsky, E. 1996 Documentation of two-dimensional impinging shock/turbulent boundary layer interaction flow. *Tech. Rep.* DLR IB 223-96 A 49, DLR Göttingen.

Schülein, E. & Trofimov, V. M. 2007 Steady longitudinal vortices in separated turbulent flows. In *Proceedings of the First CEAS European Air and Space Congress*, CEAS-Paper 2007-116, pp. 251–260. DGLR/CEAS.

Simeonides, G. 1993 Hypersonic shock wave boundary layer interactions over simplified deflected control surface configurations. *Tech. Rep.* AGARD-R-792, Special Course on Shock-Wave/Boundary-Layer Interactions in Supersonic and Hypersonic Flows, pp. 7-1–7-47.

Tomkins, C. D. & Adrian, R. J. 2003 Large scale motions in a supersonic turbulent boundary layer. *J. Fluid Mech.* **490**, 37–74.

Trofimov, V. M. & Shtrekalkin, S. I. 1990 Longitudinal vortices and heat transfer in reattached shear layer: separated flows and jets. In *IUTAM Symposium,* Novosibirsk, Russia, pp. 417–420, Springer.

Van Driest, E. R. & Blumer, C. B. 1962 Boundary-layer transition at supersonic speeds: three-dimensional roughness effects (spheres). *J. Aerosp. Sci.* **29**, 909–916.

Vermeulen, J. P. & Simeonides, G. 1992 Parametric studies of shock wave boundary layer interactions in two-dimensional compression corners at Mach 6. *Tech. Rep.* VKI TN 181, VKI.

Zheltovodov, A. A., Pavlov, A. A., Schülein, E. & Yakovlev, V. N 1985 Interconnection chip between the flow separation and the direct and inverse transition at supersonic speed conditions: laminar–turbulent transition. In *IUTAM Symposium,* Novosibirsk, Russia, pp. 503–508, Springer.